RSC Advances

ROYAL SOCIETY OF CHEMISTRY

www.rsc.org/advances

Contents entry

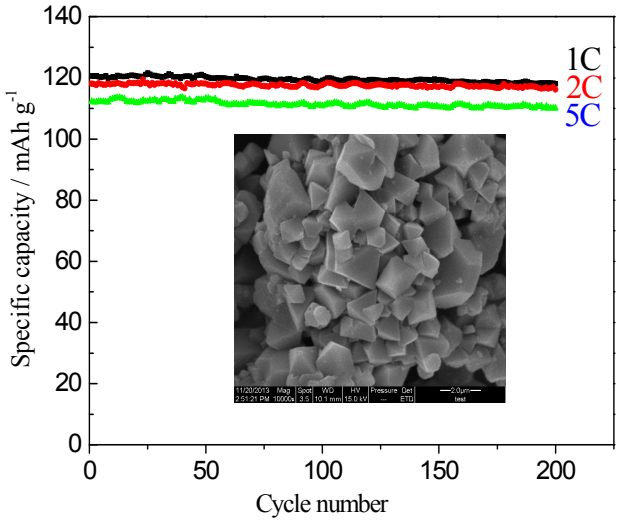

The high-voltage $LiNi_{0.5}Mn_{1.5}O_4$ synthesized at 850 °C for 12 h and sintered at 600 °C for 6 h exhibits excellently cycling stability from industrial raw materials in bulk scale (>0.5 kg).

Electrochemical properties of high-voltage $LiNi_{0.5}Mn_{1.5}O_4$ synthesized by solid-state method

Yan-Zhuo Lv [1]*, Yan-Zhang Jin [1], Yuan Xue [2], Jin Wu [3], Xiao-Gang Zhang [3] and Zhen-Bo Wang [2]*

[1] College of Material Science and Chemical Engineering, Harbin Engineering University, Harbin, 150001 China,

[2] School of Chemical Engineering and Technology, Harbin Institute of Technology, No. 92 West-Da Zhi Street, Harbin, 150001 China

[3] Xi'an Huijie Industrial Co., Ltd., Xi'an, 710116 China

*To whom all the correspondence should be addressed. E-mail:

lvyanzhuo@hrbeu.edu.cn(Y.Z.Lv), *wangzhb@hit.edu.cn* (Z.B *Wang)*

Abstract: $LiNi_{0.5}Mn_{1.5}O_4$ cathode material has been synthesized by a solid-state reaction designedly using industrial raw materials (Li_2CO_3, NiO and electrolytic MnO_2) in bulk scale, which are all without further purification. The aim is to find the optimal preparation process of $LiNi_{0.5}Mn_{1.5}O_4$ material for commercial application. The synthesis temperatures are adjusted to form disorder Fd-3m structure at 800-950 °C for 12 h and then at 600 °C for 6 h. Meanwhile, some powders have also been calcined at 850 °C for 8-14 h and next annealed at 600 °C for 6 h. XRD patterns, SEM micrographs and distribution curves of particle size give that the $LiNi_{0.5}Mn_{1.5}O_4$ cathode material calcined at 850 °C for 12 h and then annealed at 600 °C for 6 h exhibits the best crystsllinity, crystal shape as well as best normal distribution. Electrochemical test shows that the

$LiNi_{0.5}Mn_{1.5}O_4$ material synthesized at 850 °C for 12 h and then annealed at 600 °C for 6 h has the highest capacity and excellent rate capability. After 200 cycles, the capacity retentions of the sample at 1, 2 and 5 C are as high as 97.8%, 98.5% and 98.0% of its initial capacities (120.8, 118.1 and 111.2 mAh g^{-1}), respectively. The fundamental findings in this work can be applied to guide the synthesis of spinel $LiNi_{0.5}Mn_{1.5}O_4$ as high performance electrode materials for lithium ion batteries, especially for industry.

1. Introduction

Li-ion batteries are considered to be a promising electric storage technology for upcoming electric vehicles (EV), hybrid electric vehicles (HEV), plug-in hybrid electric vehicles (PHEV) and renewable energy power stations. Several research groups have reported that transition metal substituted spinel materials ($LiM_xMn_{2-x}O_4$, M=Ni, Cr, Co, Fe, Cu) are superior to $LiMn_2O_4$ due to the high-voltage plateaus above 4.5 V, namely, the so-called 5V spinels [1-5]. Among these cathode materials, $LiNi_{0.5}Mn_{1.5}O_4$ has received great attention owing to its good electrochemical performance, large energy densities and high operating voltage around 4.7 V [6-8].

Recently, a variety of synthetic methods for preparation of $LiNi_{0.5}Mn_{1.5}O_4$ material have been developed, including solid state reaction [6, 9], emulsion drying method [8], co-precipitation method [10, 11], sol-gel method [12, 13], spray pyrolysis method [14, 15], electrophoretic deposition method [16], pulsed laser deposition method [17] and solution evaporation method [18] and. Although

$LiNi_{0.5}Mn_{1.5}O_4$ as a cathode material for lithium-ion batteries with good electrochemical performances may be synthesized by these methods, there are some unfavorable factors with the high cost of raw materials or the complex process in preparation for commercial production.

Generally, the raw materials applied to solid state reaction are relatively large particles and irregular morphology. More importantly, the $LiNi_{0.5}Mn_{1.5}O_4$ particles are binary oxides, leading to the fact that it is difficult for them to be uniform mixture in the atomic level, whereby there is the discharge capacity in the 4.0 V discharge voltage plateau. In practice, Due to its simple process, low requirement of equipment, easy to industrialize, low cost and easy to control synthesis, it considered one of the most promising method to synthesize $LiNi_{0.5}Mn_{1.5}O_4$ from the business perspective. In the present paper, we use a simple and environmental friendliness method denoted as a solid-state process to synthesize half a kilo of $LiNi_{0.5}Mn_{1.5}O_4$ material (each sample) for lithium ion batteries. To the best of our knowledge, this is the first report on the preparation process and electrochemical properties of $LiNi_{0.5}Mn_{1.5}O_4$ obtained by industrial method and raw materials in bulk scale (> 0.5 kg).

2. Experimental

2.1. Material preparation

In this work, $LiNi_{0.5}Mn_{1.5}O_4$ materials were synthesized by traditional solid-state method. In detail, stoichiometric amounts of the corresponding Li_2CO_3 (99.5%, Tianqi Lithium Industries Co., Ltd), NiO (Ni content of 70.2%, Tianjin

Guanfu Institution) and electrolytic MnO_2 (Mn content of 59.6%, Guizhou Hongxing Industries Co., Ltd) precursors were mixed using a ball-mill for 1 h, and then the mixtures were put into a furnace to accomplish two-step calcinations (First step: 800-950 °C for 8-14 h, Second step: 600 °C for 6 h), where the cooling rate was 0.5 °C min^{-1} from 800-950 °C to 600 °C in flowing air atmosphere. In the following step, the samples were naturally cooled to room temperature, yielding dark powders for use. For convenience, the samples were remarked as P-800, P-850, P-900, P-950, S-8, S-10, S-12 and S-14, respectively.

2.2. Characterization of material

Powder X-ray diffraction (XRD) patterns of the samples were collected with Cu Kα radiation and recorded with a step of 0.05°. The diffraction patterns were recorded at room temperature in the 2θ range from 10° to 80°. The particle morphology of the powders after sintering was observed with a Quanta-200T scanning electron microscope (SEM). The particle size distribution was analyzed by Laser Particle Size Analyzer (PSD, LS 230, U.S. BECKMAN COULTER).

2.3. Electrochemical performance measurements

To ensure the reliability on the test results of high voltage spinel, the electrolyte was 1 mol L^{-1} $LiPF_6$ in a mixture of ethylene carbonate (EC)-dimethyl carbonate (DMC) (1:1, v/v). The $LiNi_{0.5}Mn_{1.5}O_4$ electrode sheets employed for electrochemical examinations were fabricated by homogeneously mixing $LiNi_{0.5}Mn_{1.5}O_4$ powders with conductive carbon (super P) and binder (PVDF) at a weight ratio of 8:1:1 in N-methyl-2-pyrrolidinone (NMP). And next the cathode

sheets were prepared by casting the slurry in Al foil and heated at 90 °C under vacuum for 12 h. The cells were assembled into CR2025 coin cells in an argon filled dry box. The charge-discharge test was completed in the voltage range from 3.50 to 4.95 V using a NEWARE BTS-5 at 25 °C. The 1 C charge current was used for each sample, and then various discharge currents (0.5 C, 1 C, 3 C, 5 C, 7 C and 10 C) were applied until the cells were discharged to their designed lower voltage limit. Before all of the electrochemical tests, the coin cells were pre-cycled for 3 cycles at 0.5 C to achieve a stable charge/discharge state. Cyclic voltammograms (CV) of the cells were measured on a CHI650D Electrochemical Workstation in the voltage range from 3.5 V to 5.0 V at the scanning rate of 0.05 mV s^{-1}. EIS tests were conducted at a 50% state of charge with an AC amplitude of 5 mV in the frequency range from 100 kHz to 0.01 Hz.

3. Results and discussion

3.1 Effect of calcination temperature on performance of $LiNi_{0.5}Mn_{1.5}O_4$ composite

X-ray diffraction patterns of the $LiNi_{0.5}Mn_{1.5}O_4$ material sintered at different temperatures (800-950°C) are displayed in Fig. 1. It can be found that all XRD patterns can be indexed in the Fd-3m space group, corresponding to a cubic spinel. As shown in Fig. 1, the diffraction peaks of $LiNi_{0.5}Mn_{1.5}O_4$ sintered at 850 °C for 12 h and then annealed at 600 °C for 6 h (P-850) are stronger and sharper than that of other samples, suggesting its higher crystallinity, which is benefit to high discharge capacity and good cyclability. Oppositely, the P-950

has the relatively weak diffraction peak intensity. This phenomenon may result from the decomposition of some $LiNi_{0.5}Mn_{1.5}O_4$ particles at 950 °C.

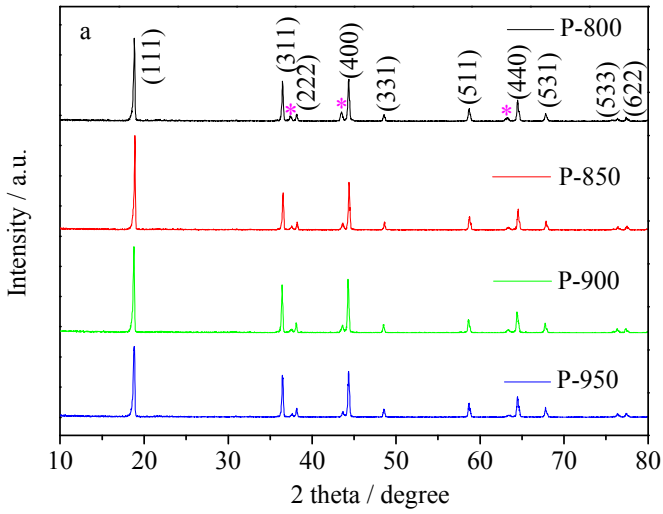

Fig. 1 XRD patterns of the $LiNi_{0.5}Mn_{1.5}O_4$ cathode powders calcined at various temperatures

As usually reported [19, 20], we can notice that four samples all have a very small amount of rock salt phase (attributed to Ni_xO or $Li_xNi_{1-X}O$ or $Li_xNi_yMn_zO$) with Bragg Peaks at 2θ = 37.4°, 43.5° and 63.2°, which can be ascribed to the oxygen deficiency in the synthesizing process. The appropriate amount existence of Mn^{3+} is in favor of better conductivity and cycling performance[21, 22].

The SEM images in Fig. 2 show the morphological changes of test samples at different calcination temperatures (800-950 °C). It can be seen that the different synthesis temperatures have a conspicuous effect on the morphology of the particle and their particle size increases with the increasing of calcination temperature. The micro-image of $LiNi_{0.5}Mn_{1.5}O_4$ obtained at 800 °C is given in

Fig. 2a. It is clear that the morphology of P-800 particles presents irregular surface appearance and severe agglomeration, suggesting low temperature has a disadvantage of taking shape for $LiNi_{0.5}Mn_{1.5}O_4$. On the contrary, Fig. 2b suggests that the $LiNi_{0.5}Mn_{1.5}O_4$ particles observed at 850 °C have well-faceted crystallized octahedral morphology, smooth surface facets and small particle size, which is in favor of the Li ion to diffuse. At the same time, When the $LiNi_{0.5}Mn_{1.5}O_4$ powders are obtained at 900 °C and 950 °C, the surface of the powders adheres to a few small particles, showed in Fig. 2c and d, which may be associated with the decomposition of some particles at high temperatures (900 °C and 950 °C).

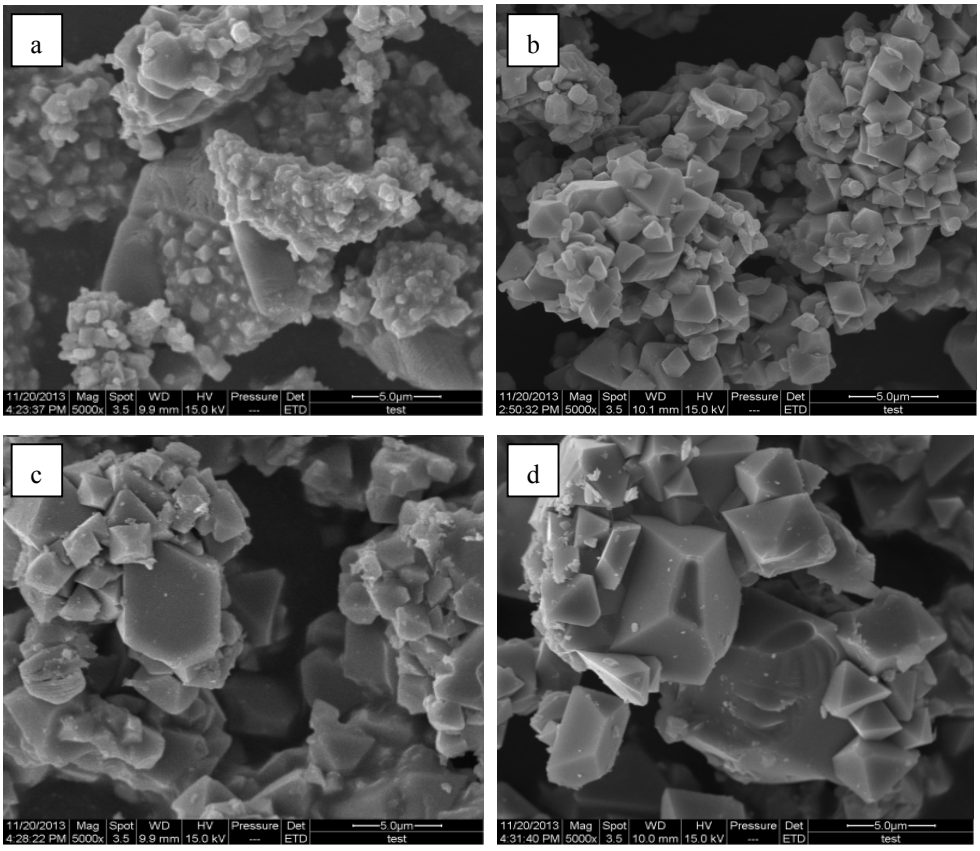

Fig. 2 SEM micrographs of the $LiNi_{0.5}Mn_{1.5}O_4$ particles calcined at various

calcination temperatures: (a) P-800; (b) P-850; (c) P-900; (d) P-950

The particle size distribution of the material obtained at different calcination temperatures is depicted in Fig. 3. As seen from the figure, the samples consist of particles in the range of 4-50 um mainly. Additionally, the particle size gradually increases with the rising of calcination temperature, which is in accordance with the result of SEM image (Fig. 2). The sample of P-850 has the best log-normal distribution with the particle mean size of 15 um.

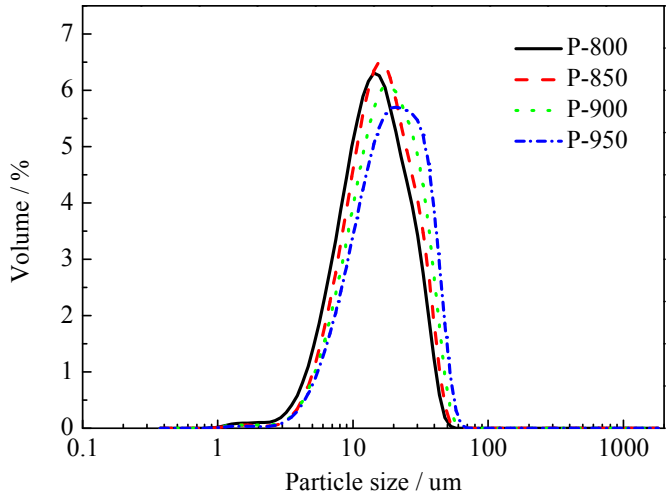

Fig. 3 Particle size distribution of P-800, P-850, P-900 and P-950 samples

Fig. 4 compares the discharge capacities of P-800, P-850, P-900 and P-950 samples at different rates and the results are shown in Fig. 4. It presents that the P-850 delivers a high capacity of 121.5 mAh g^{-1} at a rate of 0.5 C, while the samples of P-800, P-900 and P-950 give relatively lower capacities of 114.1, 118.3 and 116.1 mAh g^{-1}, respectively. Furthermore, when the C-rate is increased from 0.5 C to 10 C, 83.0% of its (P-850) initial capacity is still retained. This is

quite remarkable. Accordingly, the powder obtained at 850 °C for 12 h and then 600 °C for 6 h has the best performance of rate. However, the capacity retention rations synthesized at other temperatures (P-800, P-900 and P-950) are 76.7%, 78.6% and 77.1%, respectively. The corresponding discharging capacity of P-850 is 100.1 mAh g^{-1} at 10 C, evidently higher than 87.6, 93.5 and 89.6 mAh g^{-1} of P-800, P-900 and P-950, respectively.

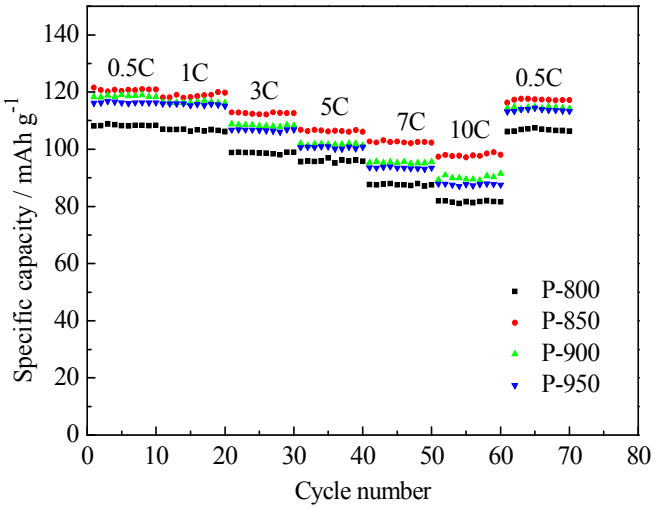

Fig. 4 Discharge capacities of P-800, P-850, P-900 and P-950 samples at different C rates

Fig. 5 displays the cycling performances of P-800, P-850, P-900 and P-950 samples. The cycling performance measurements show that the rates of 1, 2 and 5 C reduce in the following order with the calcination temperature: P-850 > P-900 > P-950 > P-800. The specific capacity of P-850 is 120.8, 118.1 and 111.2 mAh g^{-1} at the 1st cycle and 118.1, 116.2 and 109.0 mAh g^{-1} after 200 cycles with approximately 0.013, 0.010, 0.011 mAh g^{-1} capacity decay at the rates of 1, 2 and

5 C per cycle, respectively.

The P-850 sample shows an improved initial capacity compared to that found in other reports [8,18,23], which suggests that the present synthesis process is effective. P-850 also shows the best electrochemical properties than those of other samples, due to the small particle size of it. The sample synthesized at 800 °C has the lowest capacity, because of the fact that it does not form an intact crystal structure, leading to increase diffusion path of Li ion. This result is in parallel with the result obtained from the powder morphology of Fig. 2a.

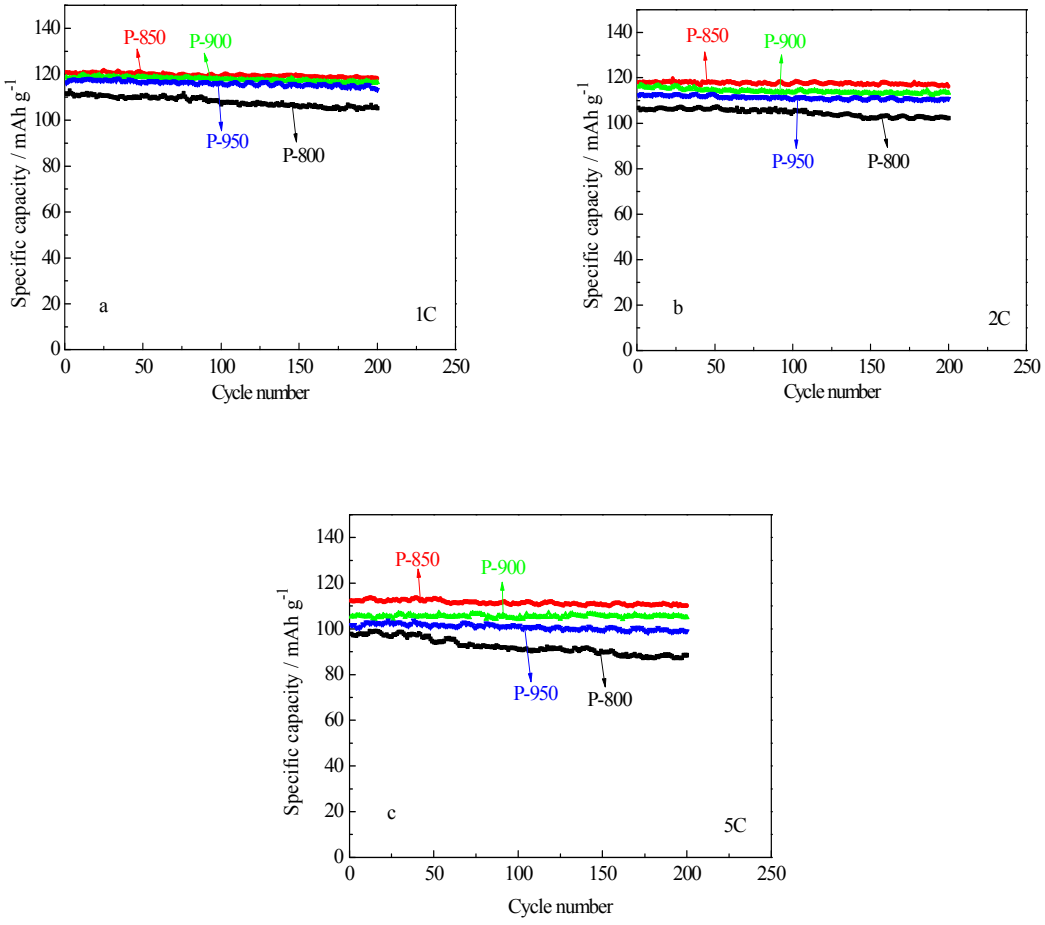

Fig. 5 Cyclic performances of P-800, P-850, P-900 and P-950 samples: (a) 1 C;

(b) 2 C; (c) 5 C

Fig. 6 exhibits the cyclic voltammetry curves of $LiNi_{0.5}Mn_{1.5}O_4$ synthesized at different temperatures (800-950 °C). The redox peaks mainly located near 4.7 V are ascribed to the two-step oxidation/reduction of Ni^{2+}/Ni^{4+} [24] or Ni^{2+}/Ni^{3+} and Ni^{3+}/Ni^{4+} [25], and small redox peaks located near 4.0 V can be attributed to the redox reaction of Mn^{3+}/Mn^{4+} couples. As shown in Fig. 6a, the 4.7 V peaks area of the P-850 is larger than those of the other samples (P-800, P-900 and P-950) before cycle, which indicates that the P-850 has a larger specific electrochemically active capacity, consistent with the analysis of Fig. 4 and Fig. 5 above. And after 200 cycles at 1 C rate, the gap between the oxidation and reduction peaks becomes large, which suggests that the electrochemical reversibility of the cells decreases. While comparing the Fig. 6a with Fig. 6b, the gap of P-850 before and after 200 cycles is smaller than other samples, meaning that P-850 delivers a more reversible redox behavior and lower polarization resistance with cycling. In addition, the small peaks at around 4.0 V attributed to the Mn^{3+}/Mn^{4+} redox couple are also observed and presented in Fig. 6a and b. The peaks area at 4.0 V of P-850 is smaller than those of P-800, P-900 and P-950, which indicates that the Mn^{3+} concentration in $LiNi_{0.5}Mn_{1.5}O_4$ of P-850 is correspondingly lower than that of other samples.

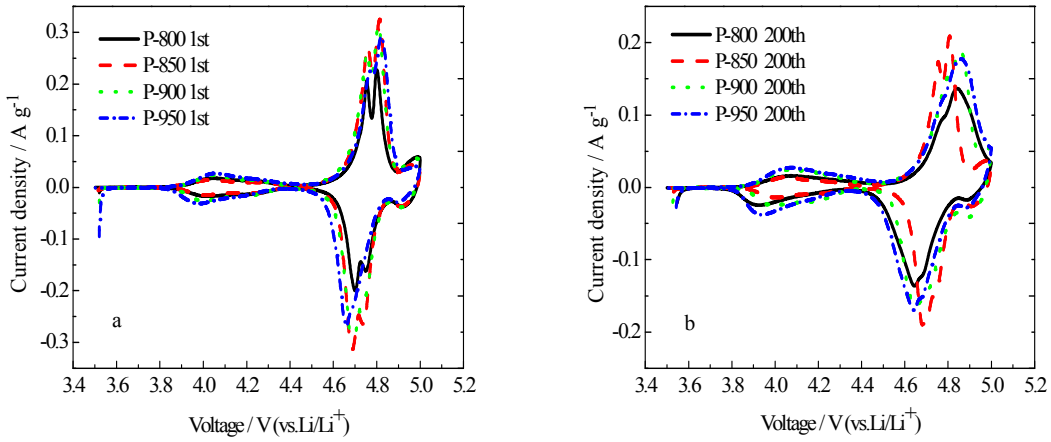

Fig. 6 Cyclic voltammetry curves of P-800, P-850, P-900 and P-950 samples: (a) after pre-cycling for 3 cycles at 0.5 C; (b) after 200 cycles at 1 C

To further elucidate the effect of calcination temperature on the electrochemical performance of $LiNi_{0.5}Mn_{1.5}O_4$ spinel, electrochemical impedance spectroscopes are described in Fig. 7. A potentiostatic step of 1-3 h is done to stabilize the potential after activating or cycling, followed by the impedance measurement that is carried out at open circuit. As shown, the EIS of the cell consists of two parts, a semicircle at high and medium frequency as well as a sloping line at low frequency. The depressed semicircle reflects the interface resistance, including surface layer as well as charge transfer reaction, and the sloping line at low frequency range is related to the solid-state diffusion of Li^+ ions in the active materials [26]. All of the samples, the impedances are small, because of the lager particle size of industrial materials, which decreases the contacting areas among particles, agreeing with the Fig. 2 and Fig. 3. With the increasing of calcination temperature (850-950 °C), the impedances of samples exhibit a similar increasing trend on cycling. Meanwhile, when the powder is

calcined at 800 °C, it has the largest impedances than others, which may be due to the serious agglomeration and irregular surface appearance of particles at low calcination temperature, resulting in increasing the diffusion path of Li^+ ions. This is consistent with the analysis of powder morphology in Fig. 2a.

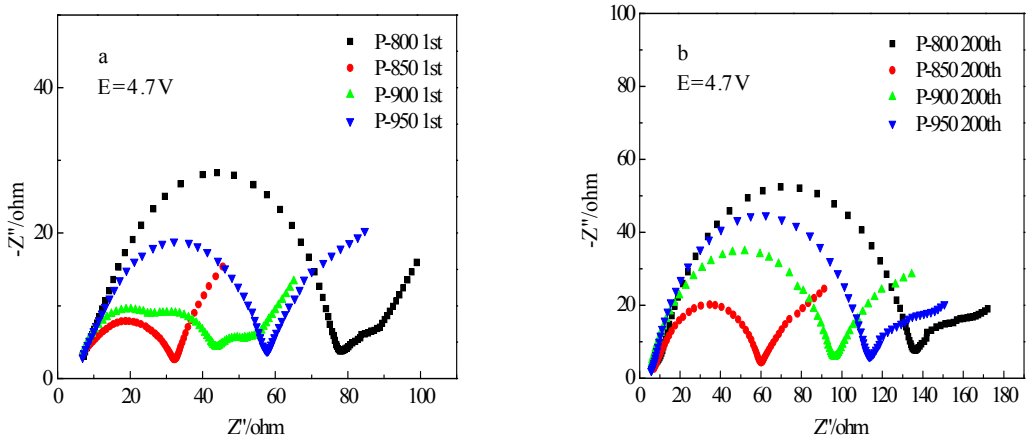

Fig. 7 Electrochemical impedance spectroscope curves of P-800, P-850, P-900 and P-950: (a) after pre-cycling for 3 cycles at 0.5 C; (b) after 200 cycles at 1 C

3.2 Effect of calcination time on performance of $LiNi_{0.5}Mn_{1.5}O_4$ composite

The XRD patterns of powders obtained at different sintering times (8-14 h) are shown in Fig. 8. All diffraction peaks also can be indexed as a cubic spinel structure and Fd-3m space group. X-ray diffraction patterns show that the peaks strength of the $LiNi_{0.5}Mn_{1.5}O_4$ powders decreases in the following order: S-12 > S-14 > S-10 > S-8. As stated above (Fig. 1), $LiNi_{0.5}Mn_{1.5}O_4$ particles synthesized at different times also display nickel oxide impurities at 2θ = 37.4°, 43.5° and 63.2°, described in Fig. 8.

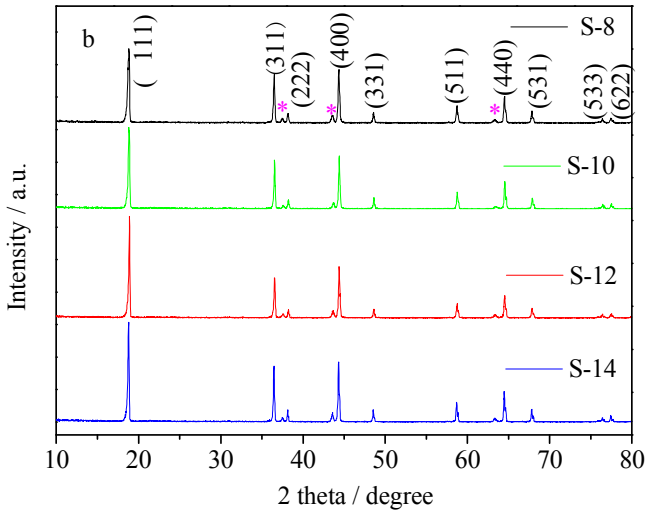

Fig. 8 XRD patterns of the $LiNi_{0.5}Mn_{1.5}O_4$ cathode powders synthesized at various times

SEM images of the $LiNi_{0.5}Mn_{1.5}O_4$ materials prepared at different calcination times are displayed in Fig. 9. It can be observed that the S-8, S-10 and S-14 powders are composed of particles of similar size. By comparing Fig. 2 and Fig. 9, it can be found that the synthesis temperature has a larger effect on morphology of material than calcination time. The SEM image of S-12 (P-850) has already been mentioned in Fig. 2b.

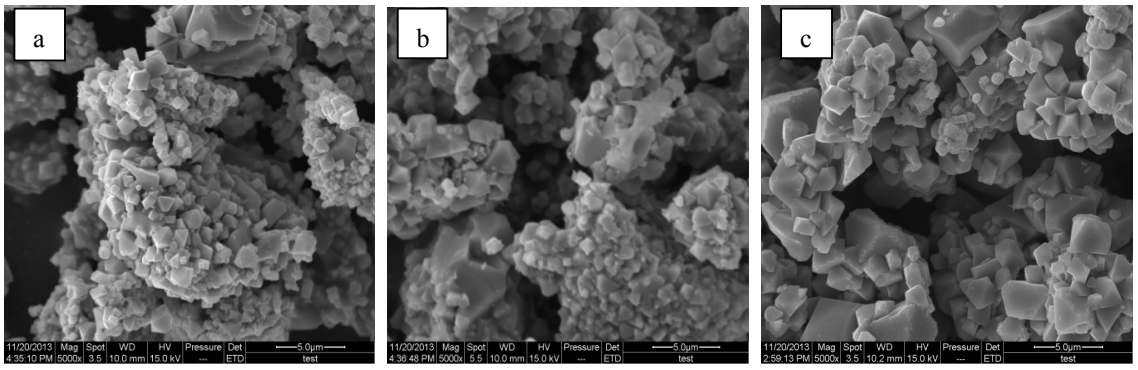

Fig. 9 SEM micrographs of the $LiNi_{0.5}Mn_{1.5}O_4$ particles synthesized at different

calcination times: (a) S-8; (b) S-10; (c) S-14

The curves of particle size distribution for S-8, S-10, S-12 and S-14 are displayed in Fig. 10. It shows that $LiNi_{0.5}Mn_{1.5}O_4$ powders synthesized at different calcination times have a similar particle size distribution. Compared with Fig. 3, it can be seen that the calcination time has a correspondingly weak influence on the curves of normal distribution. However, there are still an unignorable proportion of particles between 2 and 4 um for the S-14, which could be attributed to disintegration of the secondary hierarchical particles in long-time sintering (14 h).

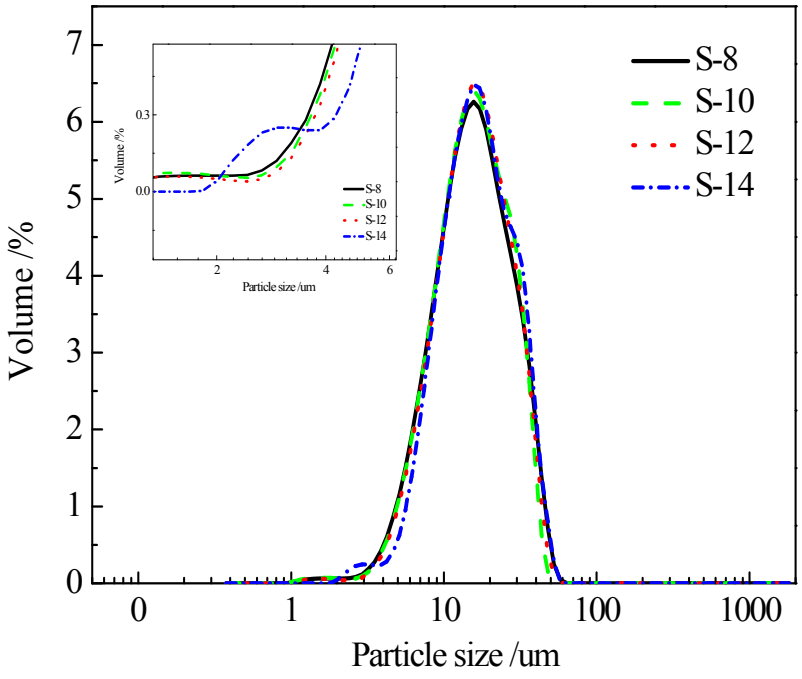

Fig. 10 Particle size distribution of S-8, S-10, S-12 and S-14 samples

The rate capability studies of spinel $LiNi_{0.5}Mn_{1.5}O_4$ synthesized at 850 °C for

8-14 h and then annealed at 600 °C for 6 h are shown in Fig. 11. As a whole, the S-12 sample exhibits a better discharge capacity than those of the S-8, S-10 and S-14 samples. When discharged at the same rate, the difference of capacity is small between each synthesis time interval (12-14 h, 14-10 h and 10-8 h). Therefore, comparing Fig. 4 with Fig. 11, it can also be demonstrated that calcination temperature has a greater influence than calcination time on the current rate of $LiNi_{0.5}Mn_{1.5}O_4$.

After high rate testing, all samples are discharged back to low C-rate (0.5 C) to test the capacity. Approximately 99% of the original capacity is retained in $LiNi_{0.5}Mn_{1.5}O_4$, which represents excellent structure integrity of all as-prepared materials and leaves no structural damages after high current cycling.

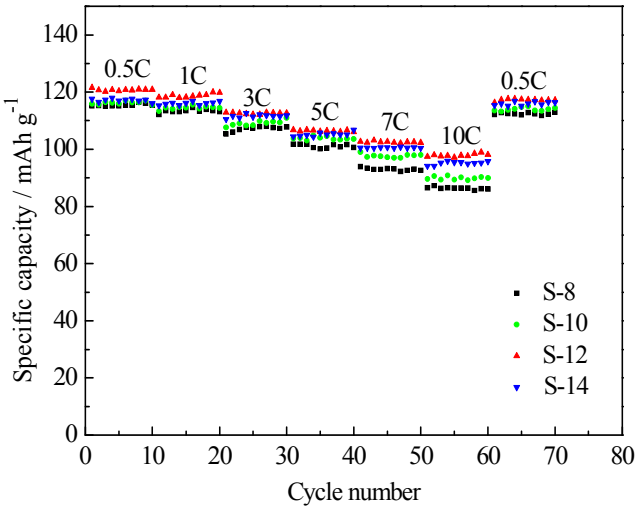

Fig. 11 Discharge capacities of S-8, S-10, S-12 and S-14 samples at different C rates

Fig. 12 illustrates cycling performances of $LiNi_{0.5}Mn_{1.5}O_4$ cathodes (S-8,

S-10, S-12 = P-850 and S-14) at 1, 2 and 5 C. The excellent cycling curves of S-12 at different rates are presented in Fig. 5. The other samples of S-8, S-10 and S-14 also exhibit identically excellent capacity retentions over 97% after 200 cycles. Meanwhile, a comparison of the result with the high rate (5 C) cycling in Fig. 12c shows that the capacity of P-850 is significantly greater than those of S-8, S-10, S-12 and S-14 in the experiment. It is demonstrated that electrochemical performances of $LiNi_{0.5}Mn_{1.5}O_4$ cathodes cycled at rates of 1 and 2 C are relatively weak effect between 8 h and 14 h, especially at 1 C. This result is consistent with the above-mentioned observation of the particle size distribution (Fig. 3 and Fig. 10).

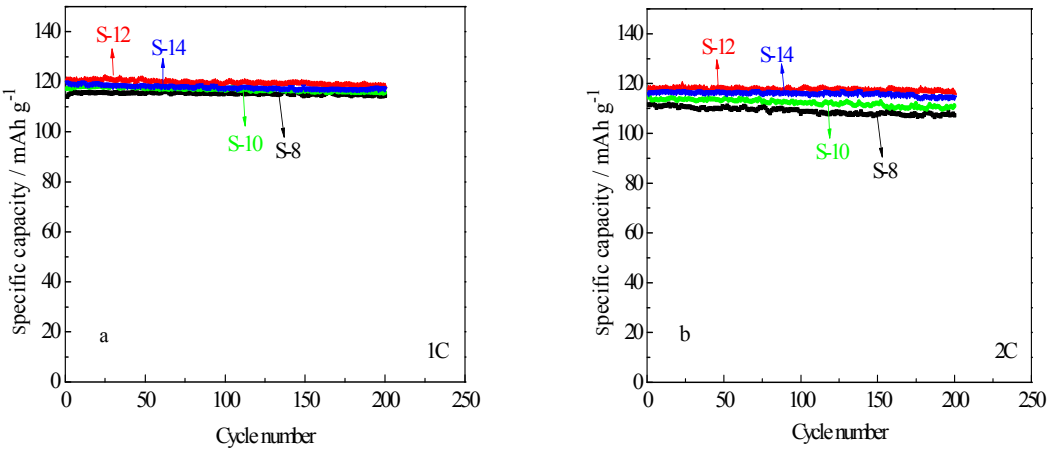

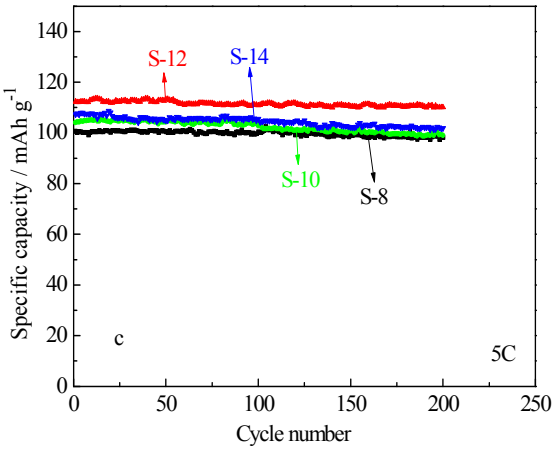

Fig. 12 Cyclic performances of S-8, S-10, S-12 and S-14 samples: (a) 1 C; (b) 2 C; (c) 5 C

Fig. 13 shows the cyclic voltammograms of the cells with the S-8, S-10, S-12 and S-14 samples as the working electrodes. On the one hand, it can be observed in Fig. 13a that the sample of S-12 (P-850) has a larger 4.7 V peaks area than that of other samples (S-8, S-10 and S-14) after pre-cycling for 3 cycles at 0.5 C, indicating that the S-12 has a larger specific electrochemically active area, consistent with the analysis of Fig. 11 and Fig. 12. On the other hand, after 200 cycles at 1 C, the difference (ΔEp) in potential between the anodic and cathodic peaks for S-12 (0.11 V, 0.03 V) is much smaller than that of S-8 (0.25 V), S-10 (0.15 V, 0.12 V) and S-14 (0.13 V, 0.08 V), indicating faster lithium insertion/extraction kinetics and higher reversibility of the electrode reaction in the former [27].

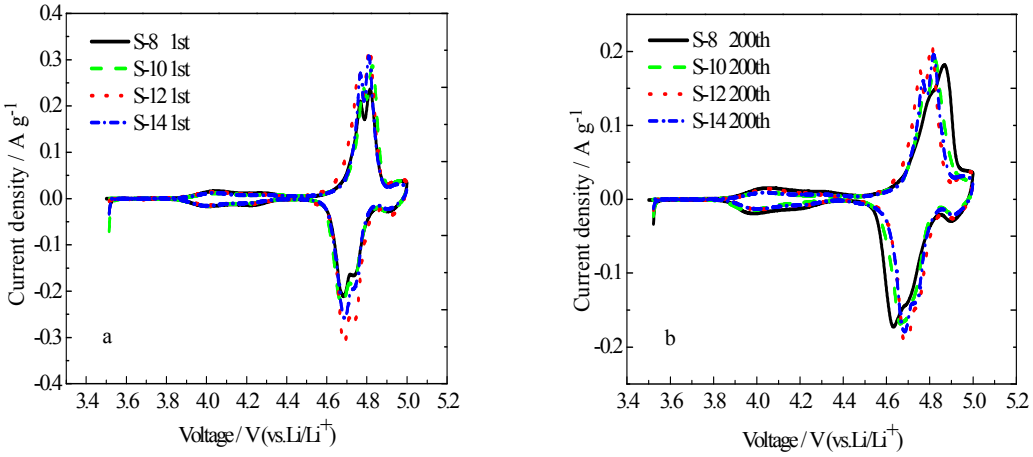

Fig. 13 Cyclic voltammetry curves of S-8, S-10, S-12 and S-14 samples: (a) after pre-cycling for 3 cycles at 0.5 C; (b) after 200 cycles at 1 C

The explanation above is in accordance with the EIS results given in Fig. 14. As can be seen in the figure, the impedance of sample obtained at 12 h (32 Ω, 60 Ω) is smaller than that of S-8 (63 Ω, 114 Ω), S-10 (55 Ω, 90 Ω) and S-14 (48 Ω, 63 Ω) before and after 200 cycles at 1 C rate. The result indicates that the polarization of electrode prepared at 850 °C for 12 h and next annealed 600 °C for 6 h is smaller during cycling, which is favorable to the cyclability.

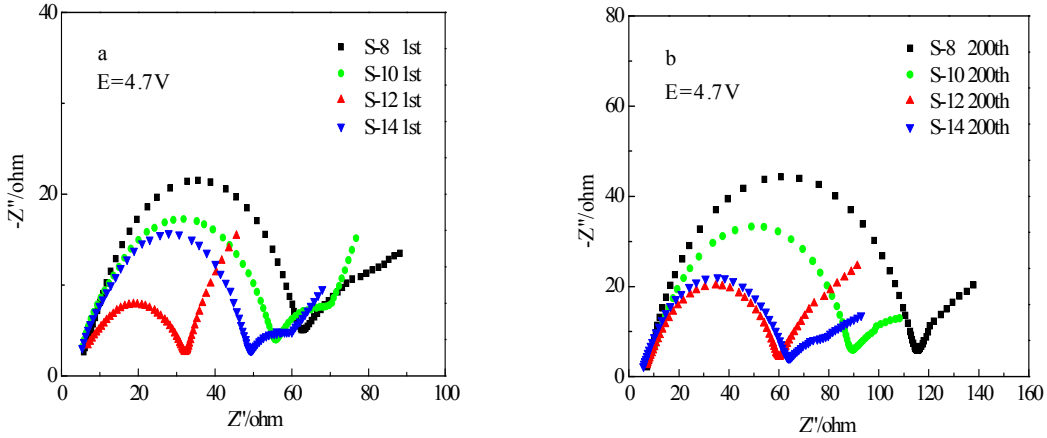

Fig. 14 Electrochemical impedance spectroscope curves of S-8, S-10, S-12 and S-14 samples: (a) after pre-cycling for 3 cycles at 0.5 C; (b) after 200 cycles at 1 C

4. Conclusion

In summary, $LiNi_{0.5}Mn_{1.5}O_4$ as a 5 V cathode material for lithium-ion battery is synthesized by solid-state method using industrial raw materials (Li_2CO_3, NiO and electrolytic MnO_2) in bulk scale. The calcination temperature has a greater influence than calcination time on the material morphology and electrochemical performance. The particles of the $LiNi_{0.5}Mn_{1.5}O_4$ spinel calcined at 850 °C for 12 h and then annealed 600 °C for 6 h have the sharper diffraction peaks and well-faceted crystallized octahedral morphology. And the discharge capacities show that the material (P-850 = S-12) delivers an initial capacity as high as 120.8, 118.1 and 111.2 mAh g^{-1} with the retentions of 97.8, 98.5 and 98.0 % after 200 cycles at 1, 2 and 5 C, respectively. Furthermore, at the rate of 10 C, the discharge capacity is significant higher than other samples. The intensive electrochemical test results of P-850 (S-12) are superior to those samples of

P-800, P-900, P-950, S-8, S-10 and S-14. Accordingly, our studies offer important benefits for $LiNi_{0.5}Mn_{1.5}O_4$ material to meet the large-scale application requirements of high-performance LIBs.

Acknowledgements

We acknowledge the National Natural Science Foundation of China (Grant No. 21273058), China postdoctoral science foundation (Grant No.2012M520731), Heilongjiang postdoctoral financial assistance (LBH-Z12089) for their financial support.

References

[1] Y. P. Fu, Y. H. Su, C. H. Lin, S. H. Wu, *J. Mater. Sci.*, 2006, **41**, 1157-1164.

[2] Y. C. Sun, Z. X. Wang, X. J. Huang, L. Q. Chen, *J. Power Sources*, 2004, **132**, 161-165.

[3] Y. -K. Sun, K. -J. Hong, J. Prakash, K. Amine, *Electrochem. Commun.*, 2002, **4**, 344-348.

[4] J. Molenda, J. Marzec, K. Swierczek, D. Palubiak, W. Ojczyk, M. Ziemnicki, *Solid State Ionics*, 2004, **175**, 297-304.

[5] Y. Ein-Eli, J. T. Vaughey, M. M. Thackeray, S. Mukerjee, X. Q. Yang, J. McBreen, *J. Electrochem. Soc*., 1999, **146**, 908-913.

[6] H. S. Fang, Z. X. Wang, X. H. Li, H. J. Guo, W. J. Peng, *J Power Sources*, 2006, **153**, 174-176.

[7] X. Wu, S. B. Kim. *J Power Sources*, 2002, **109**, 53-57.

[8] S. T. Myung, S. Komaba, N. Kumagai, H. Yashiro, H. T. Chung, T. H. Cho,

Electrochim. Acta, 2002, **47**, 2543-2549.

[9] Z. Chen, H. Zhu, S. Ji, V. Linkov, J. Zhang, W. Zhu, *J. Power Sources*, 2009, **189**, 507-510.

[10] H. B. Kang, S. T. Myung, K. Amine, S. M. Lee, Y. K. Sun, *J. Power Sources*, 2010, **195**, 2023-2028.

[11] Y. S. Lee, Y. K. Sun, S. Ota, T. Miyashita, M. Yoshio. *Electrochem Commun.*, 2002, **4**, 989-994.

[12] T. Yang, N. Zhang, Y. Lang, K. Sun, *Electrochim. Acta*, 2011, **56**, 4058-4064.

[13] H. Liu, Y. P. Wu, E. Rahm, R. Holze, H. Q. Wu, *J Solid State Electrochem.*, 2004, **8**, 450-466.

[14] S. H. Park, Y. K. Sun. *Electrochim Acta,* 2004, **50**, 431-434.

[15] D. Li, A. Ito, K. Kobayakawa, H. Noguchi, Y. Sato, *Electrochim Act*a, 2007, **52**, 1919-1924.

[16] A. Caballero, L. Hernan, M. Melero, J. Morales, R. Moreno, B. Ferrari, *J Power Sources*, 2006, **158**, 583-590.

[17] H. Xia, S. B. Tang, L. Lu, Y.S. Meng, G. Ceder, *Electrochim Acta*, 2007, **52**, 2822-2828.

[18] Y. C. Dong, Z. B. Wang, H. Qin, X. L. Sui, *RSC Adv*., 2012, **2**, 11988-11992.

[19] D. Pasero, N. Reeves, V. Pralong, A. R. West, *J. Electrochem. Soc*., 2008, **155**, A282-A291.

[20] L. Wang, H. Li, X. Huang, E. Baudrin, *Solid State Ionics*, 2011, **193**, 32-38.

[21] K. M. Shaju and P. G. Bruce, *Dalton Trans*., 2008, **40**, 5471-5475.

[22] J. H. Kim, S. T. Myung, C.S. Yoon, S. G. Kang, Y. K. Sun, *Chem. Mater*., 2004, **16**, 906-914.

[23] Z. Zhu, H. Yan, D. Zhang, W. Li, Q. Lu, *J. Power Sources*, 2013, **224**, 13-19.

[24] T. Yang, N. Zhang, Y. Lang, K. Sun, *Electrochim. Acta*, 2011, **56**, 4058-4064.

[25] B. Markovsky, Y. Talyossef, G. Salitra, D. Aurbach, H. -J. Kim, S. Choi, *Electrochem. Commun*., 2004, **6**, 821-826.

[26] D. Aubarch, *J. Power Sources*, 2000, **89**, 206-218.

[27] Y. J. Zhu, C. S. Wang, *J. Phys. Chem. C*, 2011, **115**, 823-832.